Sensorless Reserved Power Control Strategy for Two-Stage Grid-Connected Photovoltaic Systems

Sangwongwanich, Ariya; Yang, Yongheng; Blaabjerg, Frede

Published in:
Proceedings of the 7th International Symposium on Power Electronics for Distributed Generation Systems (PEDG), 2016

DOI (link to publication from Publisher):
10.1109/PEDG.2016.7527032

Publication date:
2016

Document Version
Early version, also known as pre-print

Sensorless Reserved Power Control Strategy for Two-Stage Grid-Connected Photovoltaic Systems

Ariya Sangwongwanich[1], Yongheng Yang[2], *IEEE Member*, and Frede Blaabjerg[3], *IEEE Fellow*

Department of Energy Technology
Aalborg University
Pontoppidanstraede 101, Aalborg, DK-9220 Denmark
ars@et.aau.dk[1], yoy@et.aau.dk[2], fbl@et.aau.dk[3]

***Abstract*—Due to still increasing penetration level of grid-connected Photovoltaic (PV) systems, advanced active power control functionalities have been introduced in grid regulations. A reserved power control, where the active power from the PV panels is reserved during operation, is required for grid support. In this paper, a cost-effective solution to realize the reserved power control for grid-connected PV systems is proposed. The proposed solution routinely employs a Maximum Power Point Tracking (MPPT) control to estimate the available PV power and a Constant Power Generation (CPG) control to achieve the power reserve. In this method, the irradiance measurements that have been used in conventional control schemes to estimate the available PV power are not required, and thereby being a sensorless solution. Simulations and experimental tests have been performed on a 3-kW two-stage single-phase grid-connected PV system, where the reserved power control is achieved.**

***Index Terms*—Active power control, reserved power control, maximum power point tracking, constant power generation control, PV systems, grid-connected power converters.**

I. Introduction

In the recent decade, the penetration level of Photovoltaic (PV) systems has been continuously increasing, especially for grid-connected applications [1]–[5]. Due to the still reduced installation costs (e.g., PV panels, inverters), PVs will have an even more significant role in the future power production [2], [3]. As a consequence, some grid regulations have recently been revised, in order to handle the increased amount of fluctuating PV power [5]–[9]. Several advanced active power control strategies have been defined [4]–[9], where the PV system is expected to be more active in the power network. One of the advanced functionalities in grid-connected PV systems is to reserve active power for potential grid voltage or frequency regulations [4], [7]–[9], where a certain amount of active power is reserved (or curtailed) during operation. Fig. 1 gives an example of the reserved power control requirement in the Danish grid code [7]. Typically, the Reserved Power Control (RPC) can be adopted for frequency regulation in a short period [6]–[11] and energy balancing in electricity market in a long period [4].

Energy storage devices (e.g., battery) are normally employed to realize the power reserve in PV systems [11]–[16]. However, high cost and limited lifetime are the two main drawbacks, which makes this solution not so cost-effective [10]. Alternatively, the power reserve can be achieved by modifying the control algorithm of the PV system to operate below the Maximum Power Point (MPP) [17]–[21]. In order to do so, the MPPT algorithm has to be modified to be able to regulate the PV power P_{pv} at a certain power limit P_{limit}, as it has been proposed in [10]–[12] and illustrated in Fig. 2. To achieve the RPC strategy, the set-point P_{limit} has to be calculated by subtracting the available PV power P_{avai} with the required amount of reserved power ΔP as

$$P_{\text{pv}} = P_{\text{limit}} = P_{\text{avai}} - \Delta P \tag{1}$$

Usually, the reserved power ΔP is calculated as a function of the frequency deviation or given by the system operators [10]–[12]. Thus, the remaining issue becomes how to accu-

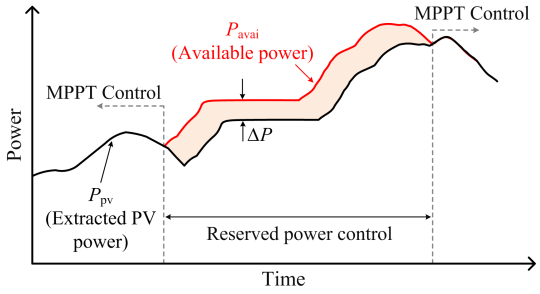

Fig. 1. Reserved power control requirement in the Danish grid code [7].

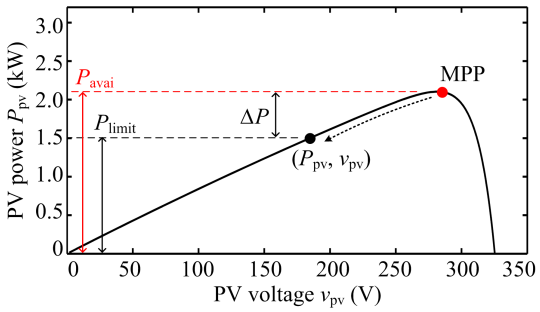

Fig. 2. Power-voltage curve of the PV panels with the reserved power control.

978-1-4673-8617-3/16/$31.00

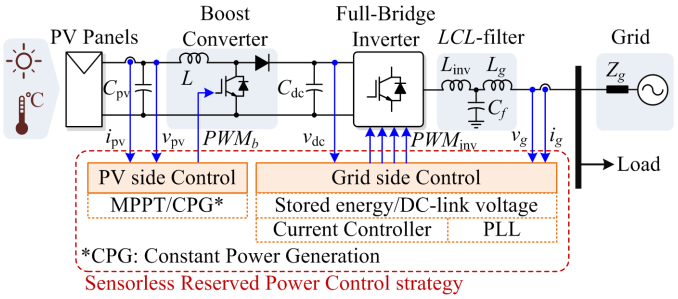

Fig. 3. System configuration and control structure of a two-stage grid-connected PV system with the Sensorless Reserved Power Control strategy.

rately estimate the available PV power P_{avai} during operation [22]. The estimation is very challenging [23], unless the PV system is equipped with an accurate irradiance measurement as implemented in [10], [11]. However, this is usually not the case for residential/commercial scale PV systems, since the irradiance measurements will increase both the cost and the complexity of the overall system. In contrast, the method proposed in [12], [23] uses a quadratic curve-fitting approach to estimate the available PV output power from the Power-Voltage (P-V) curve, without using an irradiance measurements. However, it requires the estimation of the PV voltage at the MPP V_{MPP}, which incurs additional efforts. Besides, the accurate estimation of the curve-fitting approach is limited to a certain range (i.e., $v_{\text{pv}} < V_{\text{MPP}}$) and the method is also sensitive to parameter variations.

In light of the above issues, there is a need for a cost-effective and simple solution to realize the RPC strategy. This paper proposes a Sensorless Reserved Power Control (SRPC) strategy, where the irradiance measurements are not required for the available PV power estimation. The proposed solution routinely employs the MPPT operation to measure the available output power, which is simple and more generic. Then, the PV output power is regulated according to the required amount of power reserve by using a CPG strategy [17], [18]. At the grid-side converter, the stored energy in the dc-link is also adaptively controlled in order to absorb the increase in the injected PV power during the MPPT operation, and thereby keep the injected ac power to follow the required power reserve profile. This approach can overcome the limitation in [24], where the RPC cannot be maintained during the MPPT operation. Simulations and experiments have been performed on a 3-kW two-stage single-phase grid-connected PV systems to verify the effectiveness of the proposed strategy.

II. Proposed Sensorless Reserved Power Control Strategy

A. System Description

The system configuration of the two-stage grid-connected PV systems is shown in Fig. 3, and the system parameters are given in Table I. This configuration is widely used in the residential/commercial PV systems [25], where it consists of two power converters: 1) the PV-side dc-dc boost converter and

TABLE I
Parameters of the Two-Stage Single-Phase PV System (Fig. 3).

PV rated power	3 kW
Boost converter inductor	L = 1.8 mH
PV-side capacitor	C_{pv} = 1000 μF
DC-link capacitor	C_{dc} = 2200 μF
LCL-filter	L_{inv} = 4.8 mH, L_{g} = 4 mH, C_f = 4.3 μF
Switching frequency	Boost converter: f_b = 16 kHz, Full-Bridge inverter: f_{inv} = 8 kHz
DC-link voltage	V_{dc} = 400-650 V
Grid nominal voltage (RMS)	V_g = 230 V
Grid nominal frequency	ω_0 = 2$\pi\times$50 rad/s

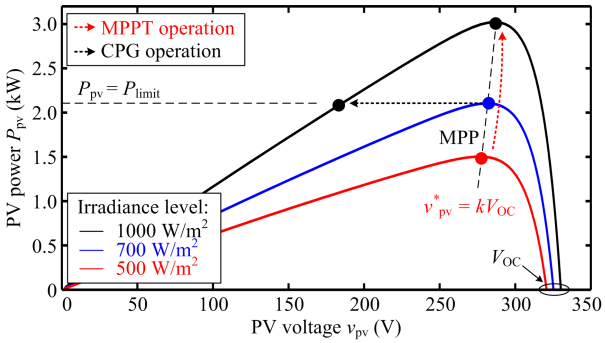

Fig. 4. Operational principle of the PV side control scheme, where the Constant Voltage MPPT and the CPG algorithms are implemented.

2) the grid-side dc-ac converter. Basically, the boost converter is responsible for extracting the PV power P_{pv}. Then, the extracted power is delivered to the ac grid by regulating the dc-link voltage v_{dc} to be constant through the control of the grid current i_{g} [26]. In fact, the stored energy in the dc-link can also be controlled at this stage.

The concept of the proposed SRPC strategy can be divided into two parts according to the power conversion stages. Ideally, the extracted power from the PV arrays P_{pv} should always follow the demand in the case of the RPC strategy shown in Fig. 1. However, it is required for the PV system to routinely operate in the MPPT mode to estimate the available power P_{avai}. During this period, the boost converter will deliver the maximum available power (i.e., $P_{\text{pv}} > (P_{\text{avai}} - \Delta P)$) to the dc-link, which violates the RPC constraint in (1). Therefore, the grid-side converter needs to minimize the power fluctuation by adaptively adjust the stored energy capacity in the dc-link in such a way to compensate for the reference grid current.

B. Control Algorithm of the PV-Side Boost Converter

At the PV-side, there are two operating modes for the boost converter. Namely, the MPPT operation is employed to estimated the available PV power, and the CPG control is employed to regulate the PV output power to follow the power reserve profile. Here, a fast MPPT operation is required in order to minimize the excessed energy injection to the dc-link during this Available Power Estimation (APE) period. A simple and effective way to operate the PV system at the MPP

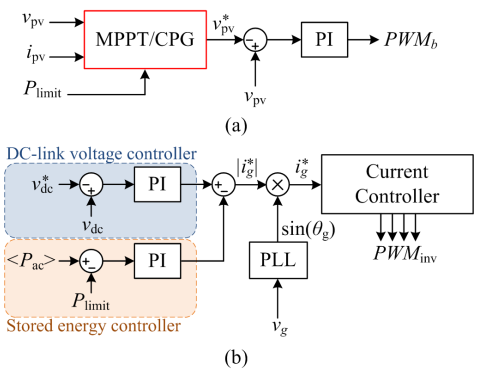

Fig. 5. Control scheme of the proposed SRPC strategy: (a) the PV-side boost converter with the MPPT and CPG operation and (b) the grid-side converter with the dc-link voltage controller and the stored energy controller.

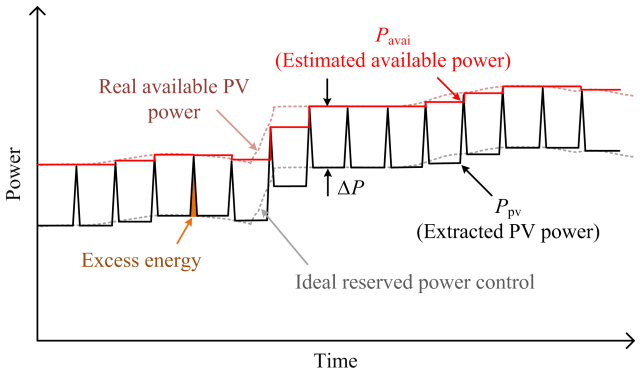

Fig. 6. The power extraction from the PV arrays according to the proposed SRPC strategy, where the MPPT operation is routinely employed for the available power estimation.

is to use a Constant Voltage MPPT (CV-MPPT) strategy, where the PV voltage v_{pv} at the MPP can be approximated as 71-78 % of the open-circuit voltage V_{OC} [27], as illustrated in Fig. 4. Since the open-circuit voltage of the PV varies in a small range during operation, the CV-MPPT method offers a fast response with a moderate accuracy, making it suitable for implementation in the proposed SRPC strategy. The reference PV voltage v_{pv}^* during the MPPT mode can be assigned as

$$v_{pv}^* = kV_{OC}, \quad 0.71 < k \leq 0.78 \tag{2}$$

where k is a constant. With the above MPPT operation, the available PV power can be estimated by simply measuring the PV power during the steady-state MPPT periods. Once the MPP is reached and the available PV power is measured, the CPG mode is assigned to the boost converter, where the operating point of the PV systems is perturbed to the left side of the MPP considering stability to achieve $P_{pv} = P_{limit}$, as it is also illustrated in Fig. 4 [17]–[19]. The reference PV voltage v_{pv}^* during the CPG mode can be summarized as

$$v_{pv}^* = \begin{cases} v_{MPPT}, & \text{when} \quad P_{pv} \leq P_{limit} \\ v_{pv} - v_{step}, & \text{when} \quad P_{pv} > P_{limit} \end{cases} \tag{3}$$

where v_{MPPT} is the reference voltage from the MPPT algorithm (i.e., the P&O MPPT) and v_{step} is the perturbation step size.

The control structure of the PV-side boost converter is shown in Fig. 5(a). By combining both MPPT and CPG operating modes, the corresponding extracted PV power from the proposed strategy can be summarized as

$$P_{pv} = \begin{cases} P_{avai}, & \text{MPPT mode} \\ P_{limit} = P_{avai} - \Delta P, & \text{CPG mode} \end{cases} \tag{4}$$

Fig. 6 further shows the power profiles at the PV side during the operation mode transitions.

C. Control Algorithm of the Grid-Side Converter

It can be noticed from (4) and Fig. 6 that the extracted PV power violates the RPC constraint during the MPPT operation. In order to minimize this power fluctuation and maintain the RPC constraint at the grid side all the time as

$$< P_{ac} >= P_{limit} = P_{avai} - \Delta P \tag{5}$$

with $< P_{ac} >$ being the averaged injected ac power, the stored energy in the dc-link should be increased during this period, in order to absorb this peak power injection. This paper employs the control scheme for the grid-side converter in Fig. 5(b), where the stored energy control is also used to calculate the reference grid current. Basically, the dc-link voltage controller will give an amplitude reference of the grid current $|i_g^*|$, which keeps the dc-link voltage v_{dc} constant and deliver all the extracted PV power to the ac grid. However, if the average injected ac power $< P_{ac} >$ starts to exceed the power limit P_{limit} (e.g., during the MPPT operation), the output of the stored energy controller will decrease $|i_g^*|$. Consequently, v_{dc} will be higher than the reference v_{dc}^* but the fluctuated power is absorbed temporarily in the dc-link. In this approach, the stored energy in the dc-link is controlled indirectly through the compensation of the grid current, which offers a faster and more effective response than the solution by directly calculating the corresponding dc-link voltage (e.g., increase v_{dc}^* during MPPT operation). This is due to the typical limited bandwidth of the dc-link voltage controller (i.e., much slower than the current controller). Notably, v_{dc} should also be within a certain range for single-phase grid-connected inverter systems, in order to ensure the power delivery to the grid and safety (e.g., 400-650 V). Thus, the stored energy controller should be deactivated when v_{dc} is outside that range, and the priority is given to the dc-link voltage regulation.

III. Design Considerations of the SRPC Strategies

In order to achieve a high control performance using the SRPC strategy, several design considerations should be discussed to assist the practical implementations.

A. Improving the Reserved Power Accuracy by Losses Compensation

So far, the efficiency of the converters are not considered. In other words, it is assumed that the PV power P_{pv} in (4) is equal to the injected ac power $< P_{ac} >$ in (5) during the RPC operation. However, there are power losses in the power converters, especially from the power devices during the switching and conduction, which reduces the converter

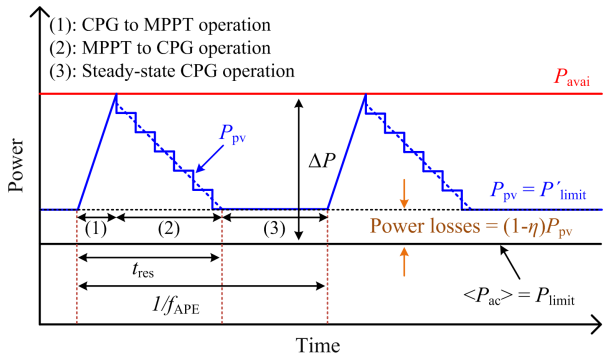

Fig. 7. Power extraction from the PV arrays according to the SRPC strategy with the power loss compensation.

efficiency. These power losses cannot be neglected and should be compensated, in order to achieve a high-accuracy operation.

Taking the efficiency of the power converter into account, the power injected to the grid from the PV arrays becomes

$$< P_{ac} > = \eta \cdot P_{pv} \quad (6)$$

$$P_{pv} - < P_{ac} > = (1-\eta) \cdot P_{pv} \quad (7)$$

where η is the efficiency of the power converter. It can be observed in (7) that there is always a certain amount of power losses from the PV side to the grid side corresponding to $(1-\eta)\cdot P_{pv}$. In order to maintain the reserved power constraint with respect to the injected ac power as in (5), the amount $(1-\eta)\cdot P_{pv}$ should be subtracted from the reference ΔP when calculating the power limit as

$$P'_{limit} = P_{avai} - [\Delta P - (1-\eta)\cdot P_{pv}] \quad (8)$$

where P'_{limit} is the compensated power limit. By replacing the P_{limit} with P'_{limit} at the PV-side controller in (4) (while (5) remains), the power losses in the power converter are compensated, as it is illustrated in Fig. 7.

B. Minimizing the Excessed Energy with the High-Performance CPG Algorithm during Transients

The key performance of the SRPC strategy is a fast operation during the available power estimation in order to minimize the excessed energy in the dc-link. Basically, there are two intermediate steps during this period: 1) CPG to MPPT transition with the CV-MPPT algorithm and 2) MPPT to CPG transition with the CPG algorithm, which are also illustrated in Fig. 7. As discussed in Section II, the former one can be achieved very fast, where the reference $v^*_{pv} = kV_{OC}$ is directly assigned. Thus, the remaining issue is to ensure a fast transient response of the CPG algorithm during the MPPT to CPG transition, which will be discussed in this part.

A simple and effective solution is to increase the perturbation step size v_{step} in such a way to improve the dynamic performance of the CPG algorithm [18]. The advantages and drawbacks of this approach are similar to those implemented in the MPPT algorithms (e.g., the P&O MPPT algorithm) [27]. For instance, a large step size can increase the tracking speed of the algorithm, but can also result in a large power oscillations during the steady-state operation. Therefore, the step size should be increased only during transients. In fact, the CPG operation employed in the proposed SRPC can be simply divided into two periods: 1) transient operation (from MPPT to CPG transition) and 2) steady-state operation (during the remaining time before the MPPT operation is assigned again), as it is also shown in Fig. 7. Thus, it is very simple to implement the modification of the step size during transients. A criterion to detect the transient operation can simply be obtained by comparing the PV power P_{pv} with the power limit P'_{limit}, and the perturbation step size can be determined as

$$v^*_{step} = \begin{cases} v_{step}, & \text{when} \quad |P_{pv} - P'_{limit}| \le \varepsilon_{ss} \\ n \cdot v_{step}, & \text{when} \quad |P_{pv} - P'_{limit}| > \varepsilon_{ss} \end{cases} \quad (9)$$

where v^*_{step} and v_{step} are the reference and the original perturbation step size, respectively. ε_{ss} is the steady-state error of the CPG algorithm due to the perturbation (e.g., 1-2 % of the rated power of the PV system) which is the criterion to determine the transient CPG operation. n is the scaling factor of the step size during the transient (e.g., n = 10). With the step size modification in (9), a large step size will be assigned only during transients to minimize the excessed energy in the dc-link, while the minimum power oscillation during the steady-state operation is maintained.

C. Maximum Sampling Frequency of the Available Power Estimation (APE) Process

The accuracy of the APE relies on its sampling frequency f_{APE}. In general, the accuracy of the APE increases as the f_{APE} increases, especially during the changing irradiance condition. However, the main constraint that limits the sampling rate of the APE is the stored energy capacity of the dc-link capacitor. This is due to the fact that during each APE process, the excessed energy will be injected into the dc-link. This time duration should be minimized as it has been discussed previously. Nevertheless, a certain time response t_{res} is required for the PV systems to change the operating mode from CPG to MPPT (to measure the available PV power) and then move back to CPG operation (to regulate the reserved power), as it is shown in Fig. 7. It should be noted that t_{res} is difficult to determine analytically due to several dependencies, e.g., power-voltage curve related to the irradiance condition (distance between the set-point P_{limit} and the MPP), the perturbation step size, the sampling rate of the CPG algorithm, and the amount of reserved power ΔP. A more practical approach is to measure t_{res} from real operation (which will be shown in Fig. 11(a)).

Once t_{res} is known, the excessed energy injected to the dc-link ΔE during each APE process can be approximated as

$$\Delta E = \frac{1}{2}(\Delta P - (1-\eta)\cdot P_{pv}) t_{res} \approx \frac{1}{2}\Delta P \cdot t_{res} \quad (10)$$

For a certain dc-link capacitor C_{dc}, the maximum energy stored in the dc-link E_{max} can be determined as

$$E_{max} = \frac{1}{2} C_{dc} (v^2_{dc,max} - v^{*2}_{dc}) \quad (11)$$

where $v_{\text{dc,max}}$ is the maximum dc-link voltage, which is normally limited by the voltage rating of the power devices and the dc-link capacitor (e.g., 650 V). v_{dc}^{*} is the reference dc-link voltage which determines the initial voltage of the dc-link. To simplify the analysis, it is assumed that the response time of the dc-link voltage controller is much slower than that of the stored energy controller, meaning that all the excessed energy is stored in the dc-link. The number of the APE process N_{APE} during the entire SRPC operation is limited to

$$N_{\text{APE}} = \frac{E_{\text{max}}}{\Delta E} = \frac{C_{\text{dc}}(v_{\text{dc,max}}^2 - v_{\text{dc}}^{*2})}{\Delta P \cdot t_{\text{res}}} \tag{12}$$

Thus, for a given operation time T, the maximum sampling frequency of the APE can be determined as

$$f_{\text{APE}} \leq \frac{N_{\text{APE}}}{T} \tag{13}$$

It is worth to mention that the actual excessed energy stored in the dc-link will be less than that in (10), since the dc-link controller will also try to regulate the v_{dc} to be constant. In that case, f_{APE} can be selected slightly higher than that in (13).

IV. Performance Verification of the Proposed SRPC Strategies

In order to verify the effectiveness of the proposed SRPC strategy, simulations have been performed on a PLECS/Simulink co-simulation platform, and the experimental tests have been carried out with the test-rig in Fig. 8, where the system parameters are given in Table I. First, a ramp changing solar irradiance profile has been used in the simulation, in order to observe the performance of the SRPC strategy during both dynamics and steady-state operation. Here, the MPPT operation is assigned to the boost converter every 0.05 s (i.e., f_{APE} = 20 Hz), as it can be seen from the PV voltage v_{pv} in Fig. 9(a). The reference ΔP is chosen as 200 W during the operation. The (real) available PV power P_{avai} and the extracted PV power P_{pv} are shown in Fig. 9(b), which demonstrates that P_{avai} is periodically measured in the MPPT mode. During the CPG operation periods, the extracted PV power P_{pv} is limited in order to follow the RPC strategy. It can be seen in Fig. 9(b) that the average ac power $< P_{\text{ac}} >$ corresponds to the extracted PV power P_{pv} during the CPG operation. This is achieved by the stored energy control, where the dc-link voltage is adaptively controlled as shown in Fig. 9(c). The reserved power ΔP can be accurately controlled during the steady-state operation (i.e., constant irradiance), as it is shown in Fig. 9(d). However, the error in ΔP increases during the changing irradiance level, due to the decrease in the accuracy of the estimated P_{avai}. It should be mentioned that the irradiance change is relatively fast in the simulation, due to the limited simulation time. Nevertheless, the results demonstrate the feasibility of the proposed SRPC strategy.

Further, the proposed SRPC strategy has also been verified experimentally with the reference ΔP of 200 W. In this case, the MPPT operation is assigned to the boost converter every 2.5 s (i.e., f_{APE} = 0.4 Hz), where the PV voltage v_{pv} is shown in Fig. 10(a). Notably, this lower sampling rate (compared to that in the simulation) is due to the fact that the sampling rate of the MPPT/CPG algorithm is chosen at 10 Hz, which is realistic [28]. Fig. 10(b) shows the (real) available PV power P_{avai}, the extracted PV power P_{pv} and the injected ac power $< P_{\text{ac}} >$ during the operation. It can be seen from Fig. 10(c) that the dc-link voltage is adaptively adjusted by the stored energy controller, in order to maintain the reserved power at 200 W as it is shown in Fig. 10(d). A zoomed-in view of the experimental results is also presented in Fig. 11. Here, the operating transition between MPPT and CPG modes can be clearly seen from the PV voltage v_{pv} in Fig. 11(a), where it can be observed that the algorithm can reach the MPP very fast with the CV-MPPT operation. The required t_{res} during the APE process is 0.5 s, as it can be measured from Fig. 11(a). It also offers a good accuracy as it can be seen from Fig. 11(b) that the peak value of the PV power P_{pv} is very close to the real available power P_{avai}. Consequently, the reserved power shown in Fig. 11(d) can accurately be controlled.

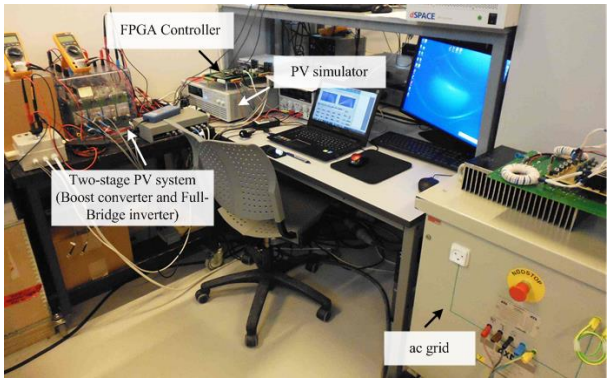

Fig. 8. Experimental setup of the two-stage grid-connected PV system.

In order to demonstrate the impact of the sampling frequency of the APE process f_{APE} to the performance of the SRPC strategy, two more simulation cases have been performed with the f_{APE} of 20 and 10 Hz, respectively. Here, the reference ΔP is selected as 500 W, which is challenging for the controller due to large injection of the excessed energy in the dc-link. Fig. 12 shows the PV power P_{pv} and injected ac power $< P_{\text{ac}} >$, where it can be seen that the APE process in Fig. 12(a) is twice as often as that in Fig. 12(b). As a result, the accuracy of the reserved power ΔP during a ramp changing irradiance condition (e.g., during 1-3 s) is higher when f_{APE} = 20 Hz, as it can be seen from Fig. 13. However, as discussed in Section III-C, the excessed energy injected into the dc-link also increases with the sampling rate f_{APE}. The dc-link voltage v_{dc} during the operation is shown in Fig. 14, where it can be clearly seen that the v_{dc} is much higher when f_{APE} = 20 Hz. In fact, the v_{dc} in Fig. 14(a) could exceed the maximum limit of 650 V at t = 2.3 s, if no action is taken (i.e., the red plot). Nevertheless, once $v_{\text{dc}} > 650$ V, the stored energy controller is deactivated, and the v_{dc} can be kept below 650 V, as it can be seen from the blue plot in Fig. 14(a).

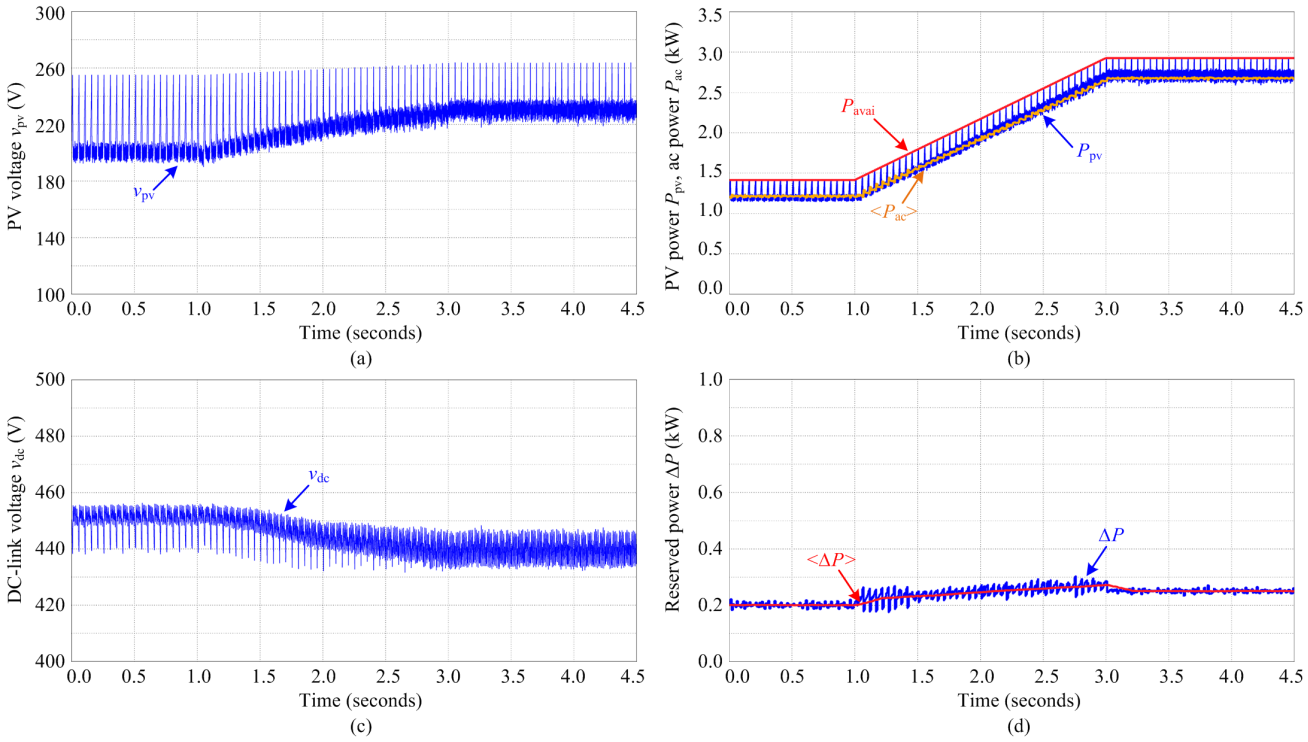

Fig. 9. Simulation results of the single-phase grid-connected PV system with the proposed SRPC strategy, where the reference ΔP is 200 W: (a) PV voltage v_{pv}, (b) PV power P_{pv} and ac power P_{ac}, (c) dc-link voltage v_{dc}, and (d) reserved power ΔP.

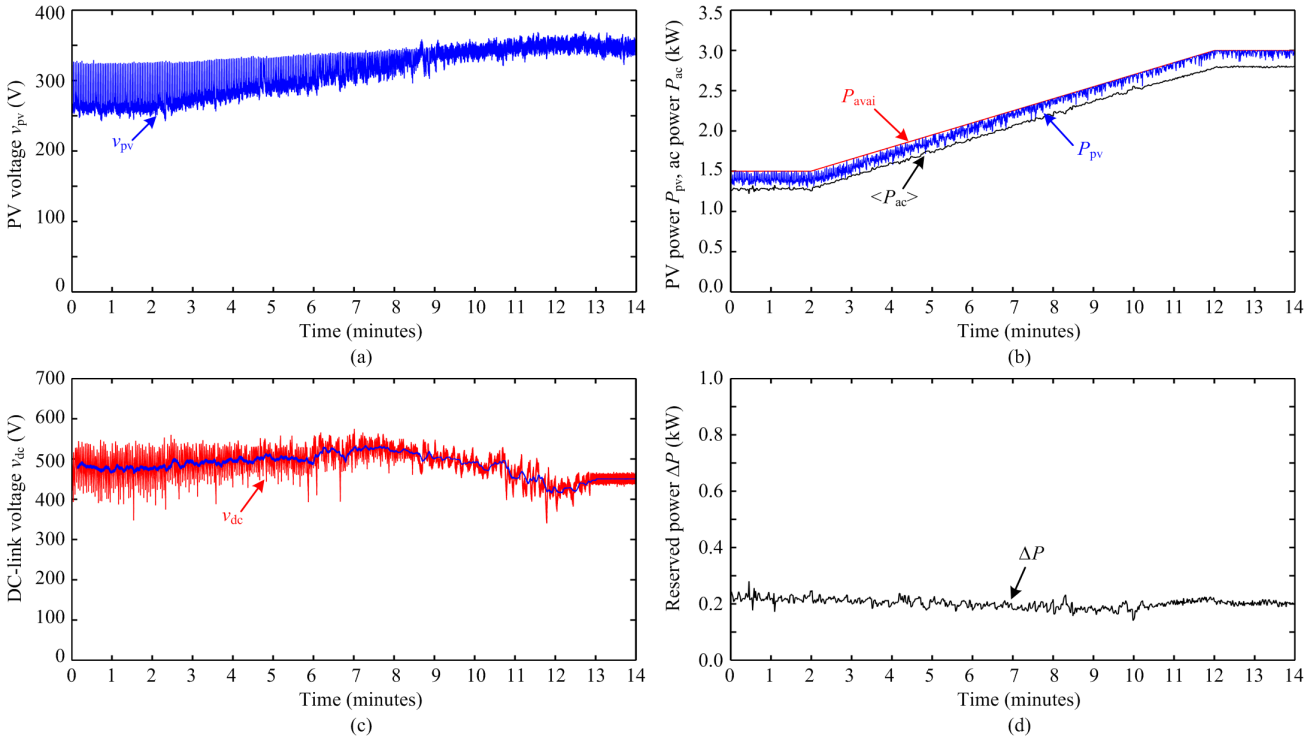

Fig. 10. Experimental results of the single-phase grid-connected PV system with the proposed SRPC strategy, where the reference ΔP is 200 W: (a) PV voltage v_{pv}, (b) PV power P_{pv} and ac power P_{ac}, (c) dc-link voltage v_{dc}, and (d) reserved power ΔP.

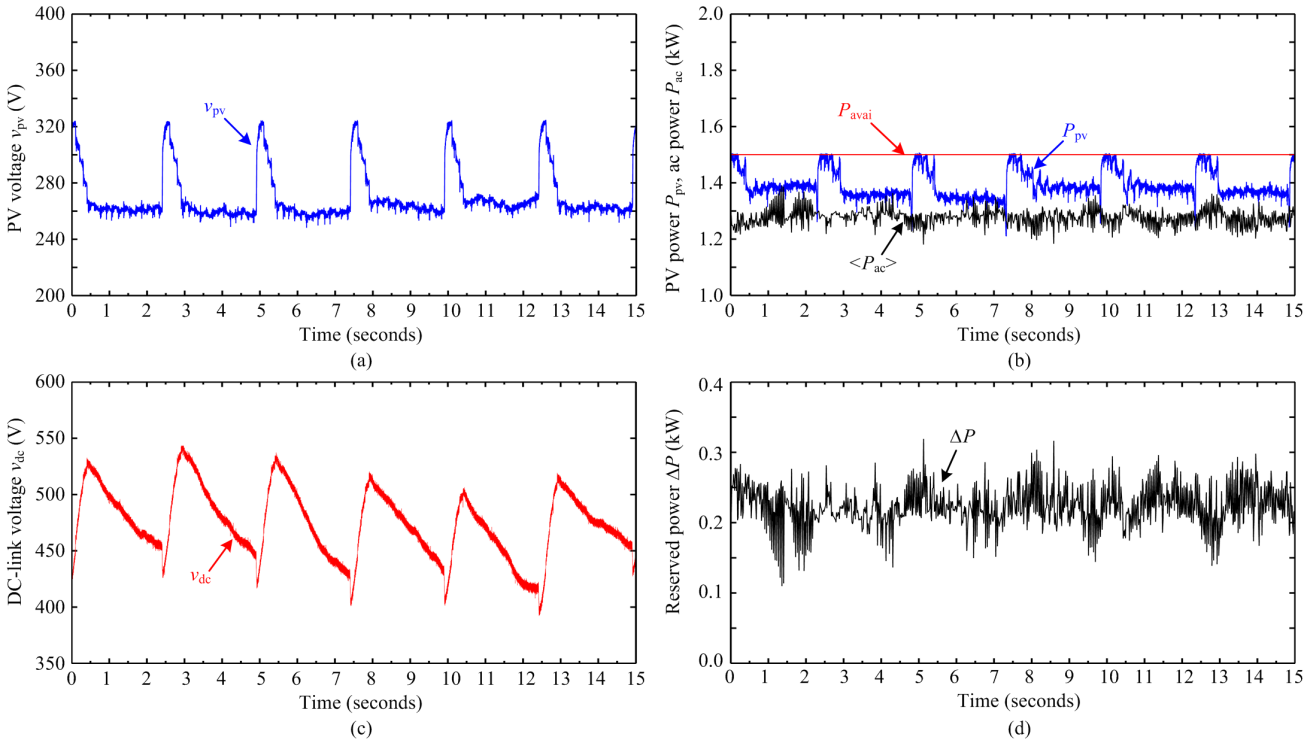

Fig. 11. Zoomed-in view of the results in Fig. 10: (a) PV voltage v_{pv}, (b) PV power P_{pv} and ac power P_{ac}, (c) dc-link voltage v_{dc}, (d) reserved power ΔP.

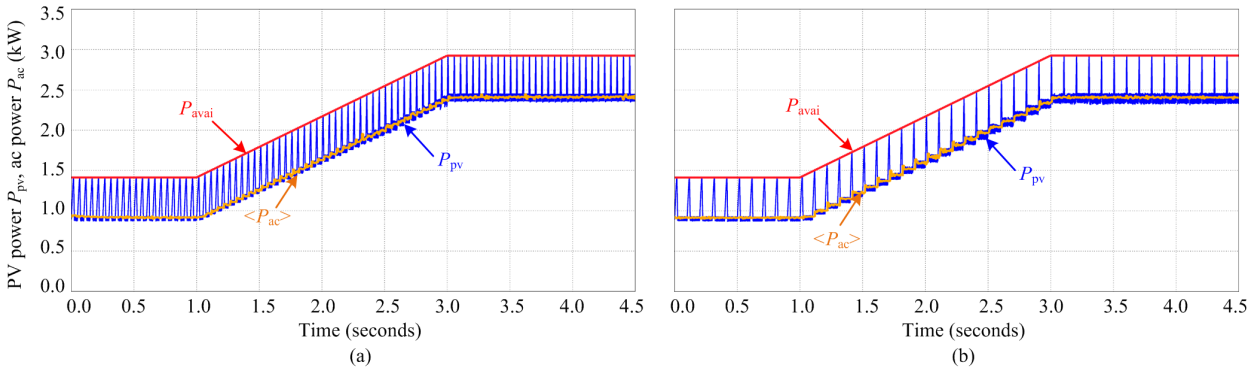

Fig. 12. Power extraction of the PV system with the proposed SRPC strategy, where the ΔP is 500 W: (a) f_{APE} = 20 Hz and (b) f_{APE} = 10 Hz.

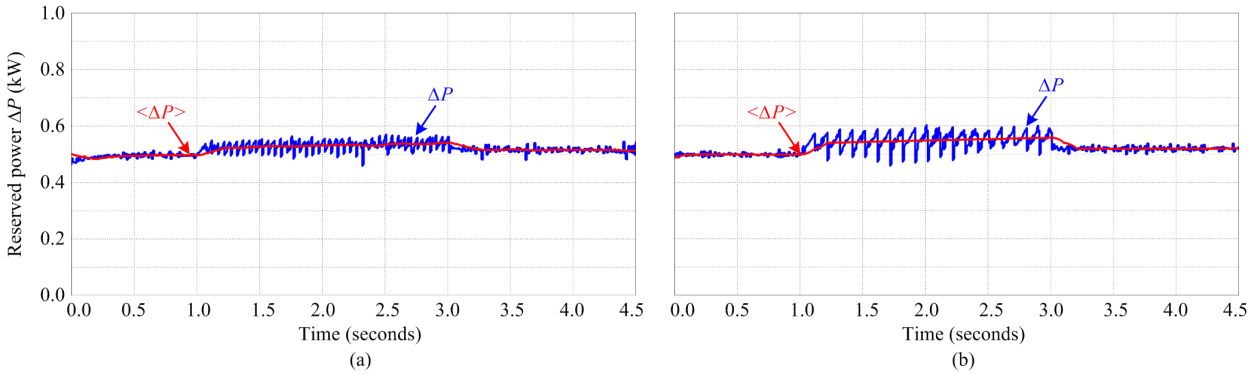

Fig. 13. Reserved power ΔP of the PV system with the proposed SRPC strategy, where the ΔP is 500 W: (a) f_{APE} = 20 Hz and (b) f_{APE} = 10 Hz.

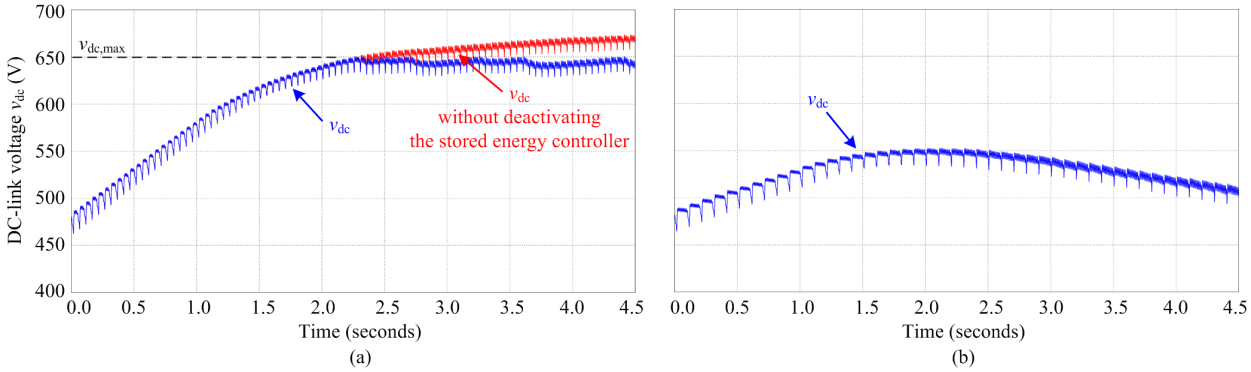

Fig. 14. DC-link voltage v_{dc} of the PV system with the proposed SRPC strategy, where the ΔP is 500 W: (a) f_{APE} = 20 Hz and (b) f_{APE} = 10 Hz.

V. Conclusion

A cost-effective sensorless reserved power control strategy for two-stage grid-connected PV systems has been proposed in this paper. The cost-effectiveness of the proposal lies in the sensorless available power estimation, which is achieved by routinely employing a fast MPPT operation. Then, the estimated available power is used for calculating the set-point to limit the extracted PV power with the CPG operation. At the grid-side, the stored energy in the dc-link is adaptively controlled to minimize the power fluctuation during the available PV power estimation process, where the excessed energy is temporarily stored in the dc-link. With the above coordinated control strategy, the reserved power control can be achieved as it has been verified in both simulations and experiments. Design considerations for a high control performance have also been discussed to assist the practical implementations.

References

[1] REN21, "Renewables 2015: Global Status Report (GRS)," 2015. [Online]. Available: http://www.ren21.net/.

[2] Fraunhofer ISE, "Recent Facts about Photovoltaics in Germany," May 19, 2015. [Online]. Available: http://www.pv-fakten.de/.

[3] Solar Power Europe, "Global Market Outlook For Solar Power 2015 - 2019," 2015. [Online]. Available: http://www.solarpowereurope.org/.

[4] National Renewable Energy Laboratory, "Industry perspectives on advanced inverters for U.S. solar photovoltaic systems: Grid benefits, deployment challenges, and emerging solutions," Tech. Rep., 2015.

[5] Y. Yang, P. Enjeti, F. Blaabjerg, and H. Wang, "Wide-scale adoption of photovoltaic energy: Grid code modifications are explored in the distribution grid," *IEEE Ind. Appl. Mag.*, vol. 21, no. 5, pp. 21–31, Sep. 2015.

[6] BDEW, "Technische richtlinie erzeugungsanlagen am mittelspannungsnetz richtlinie fur anschluss und parallelbetrieb von erzeugungsanlagen am mittelspannungsnetz," Jun. 2008.

[7] Energinet.dk, "Technical regulation 3.2.2 for PV power plants with a power output above 11 kW," Tech. Rep., 2015.

[8] E. Troester, "New German grid codes for connecting PV systems to the medium voltage power grid," in *Proc. 2nd Int. Workshop Concentrating Photovoltaic Power Plants: Opt. Design, Prod., Grid Connection*, 2009.

[9] B. I. Craciun, T. Kerekes, D. Sera, and R. Teodorescu, "Overview of recent grid codes for pv power integration," in *Proc. OPTIM*, pp. 959–965, May 2012.

[10] A. Hoke, E. Muljadi, and D. Maksimovic, "Real-time photovoltaic plant maximum power point estimation for use in grid frequency stabilization," in *Proc. COMPEL*, pp. 1–7, July 2015.

[11] B. I. Craciun, T. Kerekes, D. Sera, and R. Teodorescu, "Frequency support functions in large PV power plants with active power reserves," *IEEE J. Emerg. Sel. Topics Power Electron.*, vol. 2, no. 4, pp. 849–858, Dec. 2014.

[12] S. Nanou, A. Papakonstantinou, and S. Papathanassiou, "Control of a PV generator to maintain active power reserves during operation," in *Proc. EU PVSEC*, pp. 4059–4063, 2012.

[13] N. Kakimoto, S. Takayama, H. Satoh, and K. Nakamura, "Power modulation of photovoltaic generator for frequency control of power system," *IEEE Trans. on Energy Conversion*, vol. 24, no. 4, pp. 943–949, Dec. 2009.

[14] H. Beltran, E. Bilbao, E. Belenguer, I. Etxeberria-Otadui, and P. Rodriguez, "Evaluation of storage energy requirements for constant production in PV power plants," *IEEE Trans. on Ind. Electron.*, vol. 60, no. 3, pp. 1225–1234, Mar. 2013.

[15] J. V. Appen, T. Stetz, B. Idlbi, and M. Braun, "Enabling high amounts of PV systems in low voltage grids using storage systems," in *Proc. EU PVSEC*, pp. 2380–2386, 2014.

[16] E. Romero-Cadaval, B. Francois, M. Malinowski, and Q. C. Zhong, "Grid-connected photovoltaic plants: An alternative energy source, replacing conventional sources," *IEEE Ind. Electron. Mag.*, vol. 9, no. 1, pp. 18–32, Mar. 2015.

[17] A. Sangwongwanich, Y. Yang, F. Blaabjerg, and H. Wang, "Benchmarking of constant power generation strategies for single-phase grid-connected photovoltaic systems," in *Proc. APEC*, pp. 370–377, Mar. 2016.

[18] A. Sangwongwanich, Y. Yang, and F. Blaabjerg, "High-performance constant power generation in grid-connected PV systems," *IEEE Trans. Power Electron.*, vol. 31, no. 3, pp. 1822–1825, Mar. 2016.

[19] L. D. Watson and J. W. Kimball, "Frequency regulation of a microgrid using solar power," in *Proc. APEC*, pp. 321–326, Mar. 2011.

[20] S. Mishra, Z. P. P, and S. P. C., "A novel controller for frequency regulation in a hybrid system with high PV penetration," in *Proc. IEEE Power Energy Soc. Gen. Meet*, pp. 1–5, July 2013.

[21] Y. Yang, H. Wang, F. Blaabjerg, and T. Kerekes, "A hybrid power control concept for PV inverters with reduced thermal loading," *IEEE Trans. Power Electron.*, vol. 29, no. 12, pp. 6271–6275, Dec. 2014.

[22] D. Premm, B. Osterkamp, J. Seidel, S. Poehling, A. Unru, and B. Engel, "The PV-Regel project development of concepts and solutions for the provision of control reserve with PV," in *Proc. EU PVSEC*, pp. 3124–3128, 2015.

[23] H. Xin, Z. Lu, Y. Liu, and D. Gan, "A center-free control strategy for the coordination of multiple photovoltaic generators," *IEEE Trans. Smart Grid.*, vol. 5, no. 3, pp. 1262–1269, May 2014.

[24] Y. T. Tan, "Impact on the power system with a large penetration of photovoltaic generation," Ph.D. dissertation, Dept. Electr. Electron. Eng., Univ. Manchester Inst. Sci. Technol., Manchester, U.K., Feb. 2004.

[25] SMA, "Medium power solutions," Sunny family 2011/2012, Tech. Rep.

[26] F. Blaabjerg, R. Teodorescu, M. Liserre, and A.V. Timbus, "Overview of control and grid synchronization for distributed power generation systems," *IEEE Trans. Ind. Electron.*, vol. 53, no. 5, pp. 1398–1409, Oct. 2006.

[27] T. Esram and P.L. Chapman, "Comparison of photovoltaic array maximum power point tracking techniques," *IEEE Trans. Energy Conversion*, vol. 22, no. 2, pp. 439–449, Jun. 2007.

[28] N. Femia, G. Petrone, G. Spagnuolo, and M. Vitelli, "Optimizing sampling rate of P&O mppt technique," in *Proc. PESC*, vol. 3, pp. 1945–1949 Vol.3, Jun. 2004.